

Enhancing the Generalization Performance and Speed Up Training for DRL-based Mapless Navigation

Wei Zhang, Yunfeng Zhang and Ning Liu

Abstract— Training an agent to navigate with DRL is data-hungry, which requires millions of training steps. Besides, the DRL agents performing well in training scenarios are found to perform poorly in some unseen real-world scenarios. In this paper, we discuss why the DRL agent fails in such unseen scenarios and find the representation of LiDAR readings is the key factor behind the agent’s performance degradation. Moreover, we propose an easy, but efficient input pre-processing (IP) approach to accelerate training and enhance the DRL agent’s performance in such scenarios. The proposed IP functions can highlight the important short-distance values of laser scans and compress the range of less-important long-distance values. Extensive comparative experiments are carried out, and the experimental results demonstrate the high performance of the proposed IP approaches.

Index Terms—motion planning, generalization capability, Deep reinforcement learning

I. INTRODUCTION

DL show great potential in mapless navigation. However, previous works mainly focus on improving the agent’s navigation performance in training scenarios [1], [2]. Accordingly, good navigation results can be achieved when the testing scenarios are similar to the training scenarios [3]. However, when tested in unfamiliar scenarios, some abnormal behaviours of the DRL agent can be observed [4], [1], [5], [6], [7]. As shown in Fig. 1, when there are no obstacles between robots and targets (marked with orange boxes), the agents choose much longer paths instead of straight lines. Besides, as shown in Fig. 1(a) and 1(b), the robot even tends to approach obstacles during the goal-reaching process. Fan et al. [7] also observe their robot wander around a nearby target instead of approaching it. The above evidence reveals the navigation agents trained with DRL may behave abnormally and is not reliable in real-world scenarios. Fan et al. [7] attribute the cause of agent’s abnormal behaviours to the learning scheme, i.e., the DRL agent fails to collect training data in some special situations, the agent has little chance to learn optimal actions in the continuous action space, and the exploration noise used in training makes it hard for the agent to learn deterministic optimal policies. Although their claims are plausible, they fail to investigate the uniqueness of DRL-based robot navigation, i.e., the input representations of LiDAR reading.

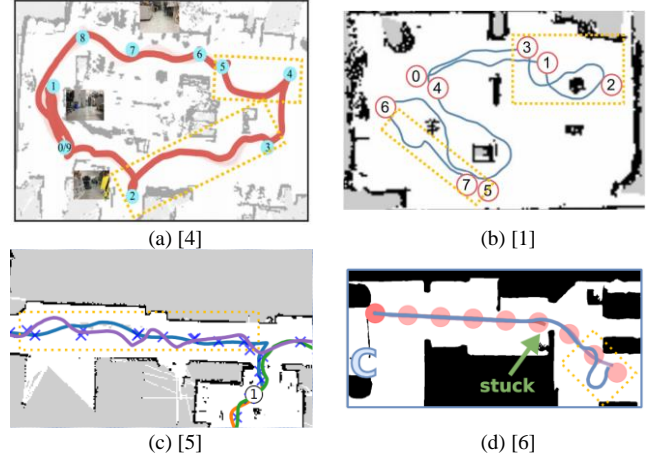


Fig. 1. Examples of abnormal behaviours learned by DRL in real-world unseen environments.

In this paper, we find the input representation of LiDAR readings is a key factor in causing the performance degradation of agent in some unseen scenarios. In most works, the input format of LiDAR readings is a vector, where each element is the distance-related value in specific direction. The distance-related value can be raw distance value [3] or min-pooled linearly normalized distance value [8], and we refer to these input representations of LiDAR readings as conventional representations. Although these representations are straightforward, they pose two problems. First, such LiDAR representations require the policy network to learn completely different policies from similar inputs. Second, the major proportion of input space is occupied by the long-distance values. Such values have less impact on obstacle avoidance, but it is necessary for the agent to collect enough training samples containing such values to enhance its generalization performance in relative open scenarios. To address the two problems, in this paper, a novel input pre-processing (IP) approach is proposed. It highlights the short-distance values in laser scans and make the policy network easier to differentiate small differences between such values. Besides, it compresses the proportion of less-important long-distance values in the input space and make the policy network easier to generalize to less-crowded scenarios. Compared to conventional input representations of LiDAR readings, the DRL agent learns much faster with the pre-processed input representations and can generalize better in unseen scenarios. To sum up, the

contributions of this paper are as follows,

- A key factor behind the performance degradation of navigation agent trained with DRL is presented.
- A novel input pre-processing approach is proposed to accelerate training and enhance the generalization capability of DRL agent.
- Extensive experiments are carried out to evaluate the high efficiency of the proposed IP approach.

II. LIMITATIONS OF CONVENTIONAL LiDAR REPRESENTATIONS

The conventional representations of LiDAR readings in previous works are vectors containing raw laser scans or linearly normalized laser scans. Without loss of generality, as shown in Fig. 2, we refer to raw LiDAR readings as $\mathbf{d} = [d_1, d_2, \dots, d_n]$, where $d_i \in [D_i^{\min}, D_i^{\max}]$ is the i -th measured distance value. To reduce the input dimension and the number of network parameters, the raw laser scans are usually compressed into m values by 1D minimum down-sampling (also called min-pooling) [8], which is as follows,

$$y_i = \min(d_{i \cdot k - k + 1}, d_{i \cdot k - k + 2}, \dots, d_{i \cdot k}) \quad (1)$$

where i is the index of the down-sampled laser scans, k is the sampling window size ($k = 0$ means min-pooling is not performed). We refer to the min-pooled input representation as $\mathbf{y} = [y_1, y_2, \dots, y_m]$. The range of y_i is $[Y_i^{\min}, Y_i^{\max}]$, where $Y_i^{\min} = \min(D_{i \cdot k - k + 1}^{\min}, D_{i \cdot k - k + 2}^{\min}, \dots, D_{i \cdot k}^{\min})$ and $Y_i^{\max} = \min(D_{i \cdot k - k + 1}^{\max}, D_{i \cdot k - k + 2}^{\max}, \dots, D_{i \cdot k}^{\max})$. In addition, we denote the linearly normalized representation of \mathbf{y} as $\mathcal{LN}(\mathbf{y}) = [\mathcal{LN}(y_1), \mathcal{LN}(y_2), \dots, \mathcal{LN}(y_n)]$, where $\mathcal{L}(\cdot): \mathbb{R} \rightarrow \mathbb{R}$ is a linear mapping.

When learning navigation skills with \mathbf{y} or $\mathcal{LN}(\mathbf{y})$ as the input representations of LiDAR readings, the DRL agent faces two challenges. First, the agent is required to generate completely different outputs on similar laser scans, which is non-trivial for deep neural networks. In LiDAR readings, the short-distance values, indicating nearby obstacles, require special attention from the agent on obstacle avoidance. A small change of such values may lead to a totally different navigation strategy. For example, as shown in Fig. 3, the laser scans in Fig. 3(a) are very similar to their counterparts in Fig. 3(b) (the

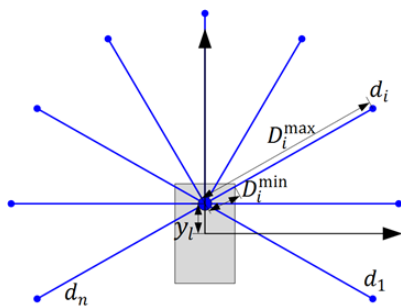


Fig. 2. Illustration of LiDAR representation for DRL-based robot navigation.

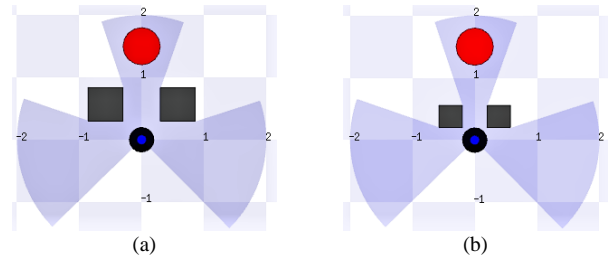


Fig. 3. Robot in two similar scenarios where the obstacle positions in both laser scans are the same. (a) the robot can move through the obstacle gate; (b) the robot cannot move through the obstacle gate.

obstacle directions in both scans are the same). If one of the observations has been collected and trained by the agent, the well-trained policy network is expected to output a similar action on the other observation during testing, because the two observations are quite similar. However, the navigation strategies for the two robots differ a lot: the first robot should move through the obstacle gate while the second one should bypass the gate. Similarly, when a robot navigates in a scenario more crowded than its training scenario, it may make wrong decisions and crash into obstacles based on the experience learned from a relatively simple scenario.

Second, the major proportion of input space of LiDAR readings is occupied by the long-distance values. Due to the high-dimensional continuous space of LiDAR observations, it is non-trivial for the agent to collect training samples covering the whole observation space during training. When encountering laser scans outside the training distribution, the agent may fail to make correct decisions. Besides, to learn good obstacle-avoidance skills, crowded scenarios are preferred for training the agent. As these scenarios are crowded, the observations received by the agent in such scenarios only contain a small partition of the full observation space. When tested in relatively open scenarios, such as an empty room, the agent's observations differ a lot from its training samples. Although the empty room is much simpler than the training scenario, the agent may still fail to perform navigation tasks in this scenario because it is unfamiliar with the received LiDAR observations.

III. PROBLEM FORMULATION

Due to the limitations of conventional input representation of laser scans, in this work, we aim to find a new input representation which can accelerate training and improve the generalization performance of the DRL agent. This problem can be modelled as a sequential decision-making process. As shown in Fig. 3, a robot is required to reach its goal position without colliding with any obstacles. It carries a LiDAR sensor on its top. The relative position of goal in robot coordinate frame $x_t^g = \{d_t^g, \varphi_t^g\}$ is assumed to be obtained by localization techniques such as sound source localization [9] or WIFI localization [10]. We denote the input of the DNN controller as $x_t = \{\mathbf{p}, x_t^g, v_t, \omega_t\}$, where \mathbf{p} is the pre-processed representation of LiDAR readings; v_t and ω_t are current linear and angular velocities of the robot. The action of the robot is

the velocity command. Given x_t , the robot takes a_t under the current policy π . It then updates the next input x_{t+1} based on new observations and receives a reward r_t calculated by the reward function. The objective of this work is to find the optimal representation \mathbf{p} that can minimize the training steps and the \mathbf{p} -conditioned optimal policy π^* that maximizes the discounted total rewards $G_t = \sum_{\tau=t}^T \gamma^{\tau-t} r_\tau$, where $\gamma \in [0,1)$ is a discount factor.

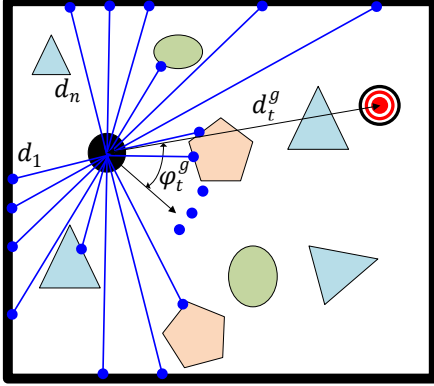


Fig. 4. Illustration of the mapless robot navigation problem.

IV. APPROACH

A. Input Pre-processing of Laser Scans

In this section, we focus on efficient input pre-processing (IP) approaches that can alleviate the adverse effects of the commonly used representations of LiDAR readings. For $\forall y_i \in \mathbf{y}$, the smaller y_i is, the closer the robot is to the obstacles and the more dangerous the current situation is. We define a threshold Y_i^C to determine whether the agent is close to obstacles in terms of the value of y_i . When $y_i < Y_i^C$, the agent is considered too close to an obstacle, and the agent must focus on obstacle avoidance. Using Y_i^C , we introduce a ratio named *PoC* (proportion of distance values considered “close”) to weigh the proportion of the “close” range on the whole measuring range of y_i and as follows,

$$\rho^{PoC}(y_i) = \left| \frac{Y_i^C - Y_i^{\min}}{Y_i^{\max} - Y_i^{\min}} \right| \quad (2)$$

It is noteworthy that the *PoC* value remains the same for the linearly normalized representations, i.e., $\rho^{PoC}(\mathcal{LN}(y_i)) = \rho^{PoC}(y_i)$. *PoC* can well reflect two characteristics of the LiDAR input. First, a small *PoC* value indicates the proportion of “close” values in y_i is small, which results in the difference between two short-distance values within the “close” range is relatively small. Second, a small *PoC* value indicates the range of “far” values in y_i is large, which means more training data containing various long-distance values are needed for maintaining the agent’s performance in relatively open scenarios. Therefore, increasing the *PoC* value can help to address two issues of conventional input representations.

To increase *PoC*, we propose an element-wise input pre-processing function $\mathcal{P}_i(\cdot): \mathbb{R} \rightarrow \mathbb{R}$, which operates on y_i , and it must satisfy the following two conditions:

- 1) $\mathcal{P}_i(y_i)$ is strictly monotonic.

$$2) \quad \mathcal{P}'_i(y_i) \mathcal{P}''_i(y_i) < 0.$$

The first condition guarantees this function is a one-to-one mapping, and the second condition ensures $\rho^{PoC}(\mathcal{P}_i(y_i)) > \rho^{PoC}(y_i)$, and the corresponding proof is as follows,

$$\begin{aligned} \rho^{PoC}(\mathcal{P}_i(y_i)) &= \left| \frac{\mathcal{P}_i(Y_i^T) - \mathcal{P}_i(Y_i^{\min})}{\mathcal{P}_i(Y_i^{\max}) - \mathcal{P}_i(Y_i^{\min})} \right| \\ &= \frac{\left| \int_{Y_i^{\min}}^{Y_i^T} \mathcal{P}'_i(\delta) d\delta \right|}{\left| \int_{Y_i^{\min}}^{Y_i^{\max}} \mathcal{P}'_i(\delta) d\delta \right|} \\ &< \frac{|\mathcal{P}'_i(Y_i^T)(Y_i^T - Y_i^{\min})|}{|\mathcal{P}'_i(Y_i^T)(Y_i^{\max} - Y_i^{\min})|} \\ &= \rho^{PoC}(y_i) \end{aligned} \quad (3)$$

As $\rho^{PoC}(\mathcal{P}_i(y_i)) > \rho^{PoC}(y_i)$, the proportion of long-distance values in the pre-processed representation $\mathcal{P}_i(y_i)$ is smaller than in the conventional representation y_i . Accordingly, fewer training samples containing long-distance values are needed. Besides, after mapped by $\mathcal{P}_i(\cdot)$, the differences between the pre-processed inputs have the following characteristics:

$$|\mathcal{P}_i(y_{i,1} + \Delta y) - \mathcal{P}_i(y_{i,1})| > |\mathcal{P}_i(y_{i,2} + \Delta y) - \mathcal{P}_i(y_{i,2})| \quad (4)$$

where $y_{i,1}$ and $y_{i,2}$ ($y_{i,1} < y_{i,2}$) are two valid distance values in y_i , Δy is the distance interval. As shown, after mapped by $\mathcal{P}_i(\cdot)$, the difference between short-distance values in y_i is expanded compared to the difference between long-distance values. Hence, it will be easier for the policy network to learn different policies from two LiDAR readings with similar small-distance values with the pre-processed representations.

Fortunately, many common functions satisfy the two conditions. In this paper, three functions, i.e., Exponential function $\mathcal{P}_i^E(\cdot)$, Reciprocal function $\mathcal{P}_i^R(\cdot)$ and Logarithmic function $\mathcal{P}_i^L(\cdot)$, as chosen as the IP function and as follows,

$$\begin{aligned} p_i^E &= \mathcal{P}_i^E(y_i) = \alpha_i^{y_i} \\ p_i^R &= \mathcal{P}_i^R(y_i) = \frac{1}{y_i - \beta_i} \\ p_i^L &= \mathcal{P}_i^L(y_i) = \ln(y_i - \gamma_i) \end{aligned} \quad (5)$$

where p_i^E , p_i^R and p_i^L denote the pre-processed value of y_i ; $\alpha_i \in (0,1)$, $\beta_i \in (-\infty, Y_i^{\min})$ and $\gamma_i \in (-\infty, Y_i^{\min})$ are hyperparameters of each function. We call $\mathbf{p} = \{p_1, p_2, \dots, p_n\}$ the pre-processed input, and the *PoC* value of p_i processed each IP function is as follows,

$$\rho^{PoC}(p_i^E) = \left| \frac{\alpha_i^{Y_i^T} - \alpha_i^{Y_i^{\min}}}{\alpha_i^{Y_i^{\max}} - \alpha_i^{Y_i^{\min}}} \right| \approx 1 - \alpha_i^{Y_i^T - Y_i^{\min}} \quad (6)$$

$$\rho^{PoC}(p_i^R) = \left| \frac{\frac{1}{Y_i^T - \beta_i} - \frac{1}{Y_i^{\min} - \beta_i}}{\frac{1}{Y_i^{\max} - \beta_i} - \frac{1}{Y_i^{\min} - \beta_i}} \right|$$

$$\approx 1 - \frac{Y_i^{\min} - \beta_i}{Y_i^T - \beta_i}$$

$$\rho^{PoC}(p_i^L) = \left| \frac{\ln(Y_i^T - \gamma_i) - \ln(Y_i^{\min} - \gamma_i)}{\ln(Y_i^{\max} - \gamma_i) - \ln(Y_i^{\min} - \gamma_i)} \right|$$

As $\alpha_i^{Y_i^{\max}}$ and $\frac{1}{Y_i^{\max} - \beta_i}$ both approach 0 with the increase of Y_i^{\max} , we replace Y_i^{\max} with 0 in calculation of $\rho^{PoC}(p_i^E)$ and $\rho^{PoC}(p_i^R)$ to reduce the influence maximum measuring range of the LiDAR.

The suitable hyperparameters (α_i , β_i and γ_i) in the IP functions can be obtained by trials and errors, which is quite time-consuming for DRL-based navigation. To avoid trials and errors, two approaches will be introduced. We can calculate the hyperparameters using a preferred *PoC* value. The preferred *PoC* value is $\frac{1}{3}$, which refers to the idea of fuzzy reactive control. In FRC, the relationships between robot and obstacles are usually classified as “very near”, “near” and “far” [11], and different navigation rules are made according to the relationships. In this thesis, the three relationships are considered equally important, and ρ^{PoC} corresponds to the proportion of distance values classified as “very near” and set as $\frac{1}{3}$ for all IP functions.

B. Automating IP Function Adjustment

In the previous section, we present several IP functions with manually given hyperparameters. Unfortunately, choosing optimal hyperparameters for those IP functions is non-trivial, and the hyperparameters calculated based on our empirical analysis may not be optimal. Instead of setting those hyperparameters manually, we can automate this procedure by treating those hyperparameters as trainable variables and learning them from training. Without loss of generality, we refer to the IP function with trainable hyperparameters as $\mathcal{P}_{\zeta_i}(\cdot)$, where ζ_i denotes trainable hyperparameters. We denote $\tilde{\theta} = \theta \cup \zeta_i$ and $\tilde{\phi} = \phi \cup \zeta_i$, and the gradient for updating the Q network and policy network can be rewritten as follows,

$$\nabla_{\tilde{\phi}} \mathcal{L}(\tilde{\phi}) = \nabla_{\tilde{\phi}} \frac{1}{|\mathcal{M}|} \sum_{(s, a, r, s', d) \in \mathcal{M}} (Q(s, a | \tilde{\phi}) - Q_{\text{target}}(s, a))^2 \quad (7)$$

$$\nabla_{\tilde{\theta}} \mathcal{L}(\tilde{\theta}) = \nabla_{\tilde{\theta}} \frac{1}{|\mathcal{M}|} \sum_{s \in \mathcal{M}} (Q(s, \tilde{a} | \tilde{\phi}) - \alpha \log \pi(\tilde{a} | s, \tilde{\theta}))^2$$

C. DRL Models

To learn navigation skills, soft actor-critic (SAC) is chosen as the DRL algorithm for training the navigation agent. To validate that the performance improvement brought by our IP approaches is irrelevant to the network structure, two DRL models with network structures presented in [8] and [4] are

utilized for training. As shown in Fig. 5 (a), the actor and critic networks of the first model are fully connected and have three hidden layers with Tanh activations. The input of actor network contains the representation of LiDAR readings and relative goal position $s_t^g = \{d_t^g, \varphi_t^g\}$. Dropout is only applied to the actor network for enhancing the generalization capability of the DRL agent [12]. As shown in Fig. 5(a), the networks of the second model are also fully connected, which have three hidden layers with ReLU activations. Different from the first model, the networks also take current velocities $\{v_t, \omega_t\}$ as input.

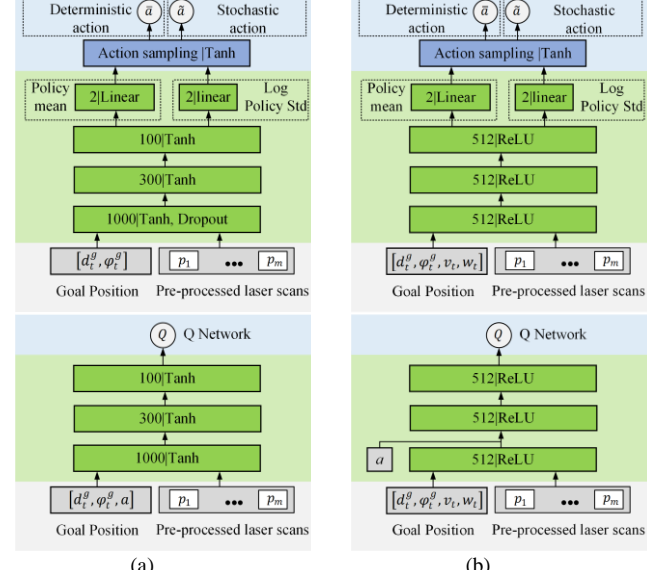


Fig. 5. Network architectures used for evaluating the efficiency of IP approaches.

V. IMPLEMENTATION AND TESTS

In this section, we evaluate our IP approaches through training robots with different shapes and LiDAR configurations in different scenarios. First, we train a circular robot with LiDAR on its top center. In this case study, the IP function keeps the same for distance values measured from all directions. Second, we train a rectangular robot with LiDAR on its front. In this case study, the IP function is unique to the distance value measured from a different direction, which is more common in real-world applications.

A. Case Study One: Circular Robot

In this case study, we evaluate our IP approaches through training a circular robot to navigate. As shown in Fig. 6, the training scenario Env_0 [8] is a $10 \times 10\text{m}^2$ room which contains a large concave region and many thin obstacles. As shown, the simulated differential robot is a circular robot with a radius of 0.2m. Its maximum linear velocity is 0.5m/s and maximum angular velocity is $\frac{\pi}{2}$ rad/s. A LiDAR is mounted on the robot center. Its FOV is 270° , angular resolution is 0.25° (1080 laser beams) and scanning range is 30m. The networks used for training the robot are given in Fig. 5(a). The input size of laser scans is reduced to 36 through min-pooling.

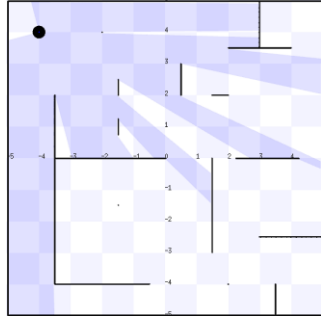


Fig. 6. Env_0: the simulated scenario used for training the circular robot.

At the beginning of each episode, the agent starts from a randomly chosen obstacle-free point and aims to reach a goal point (not rendered). Within the first 100 episodes, it takes random actions for exploration. Afterwards, it takes the stochastic action sampled from squashed Gaussian policy generated by the policy network. Each episode will terminate once the robot reaches its goal, hits obstacles, or times out (the maximum time steps per episode is 200). The publishing frequency of control command is 5Hz. We train the model in 100k steps and test the model every 5k training steps, and the size of the replay buffer is 100k. The scenarios used for testing contain the training scenario (Env_0) and three unseen scenarios (Env_1, Env_2, and Env_3) shown in Fig. 7. In each scenario, fifty start and goal points are randomly sampled from the obstacle-free regions, and the agent needs to perform the fifty goal-reaching tasks during testing.

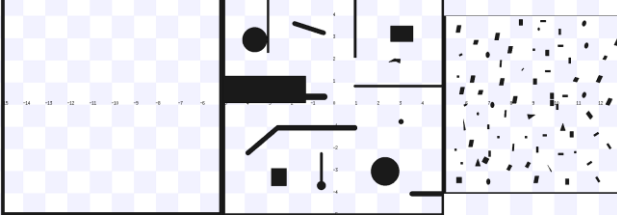


Fig. 7. The simulated scenarios used for testing, namely Env_1, Env_2, and Env_3 (left to right).

In this case study, we evaluate three input pre-processing approaches introduced in Section IV-A, namely i) IP-Exp: Exponential function $\mathcal{P}^E(\cdot)$, where $\alpha_i = 0.017$ and $\rho^{Poc}(p_i^E) \approx 1/3$; ii) IP-Rec: Reciprocal function $\mathcal{P}^R(\cdot)$, where $\beta_i = 0$ and $\rho^{Poc}(p_i^R) \approx 1/3$; iii) IP-Log: Logarithmic function $\mathcal{P}^L(\cdot)$, where $\gamma_i = 0.192$ and $\rho^{Poc}(p_i^L) = 1/3$. We remove the subscript “ i ” from each IP function $\mathcal{P}(\cdot)$ to show that the IP function keeps the same for distance values measured from all directions because the Y_i^{\min} and Y_i^{\max} are the same for all “ i ”. In addition, we compare our IP approaches with iv) Raw: raw LiDAR readings as input (named Raw); v) LNorm-v1: Linearly normalized LiDAR readings as input adopted in [8], which is as follows,

$$\mathcal{LN}^{v1}(y_i) = 2 \cdot \left(1 - \frac{\min(y_i, Y^{\max})}{Y^{\max}} \right) - 1 \quad (8)$$

where Y^{\max} ($Y^{\max} = 20$ m in this experiment) is manually given instead of directly using the maximum measuring range of LiDAR. It is noteworthy that LNorm-v1 is also applied to the

relative goal position, and hence we replace d_t^g with $\mathcal{LN}^{v1}(d_t^g)$ in our LNorm-v1 implementation.

Each model is trained five times using different random seeds, and the metric used to evaluate the model’s performance is the success rate of 50 runs in each scenario. The average learning curves are given in Fig. 8. As shown, all three IP approaches outperform the conventional approaches in terms of success rate and learning speed. Among the three IP approaches, IP-Rec performs the best in all scenarios: it achieves the highest success rate and learns the fastest compared to other approaches. It exhibits a great advantage in the scenario (Env_3) which is much more crowded than the training scenario. It is noteworthy the agents trained with conventional input representations even cannot complete all goal-reaching tasks in the empty scenario Env_1, which is in accordance with the observations in [7].

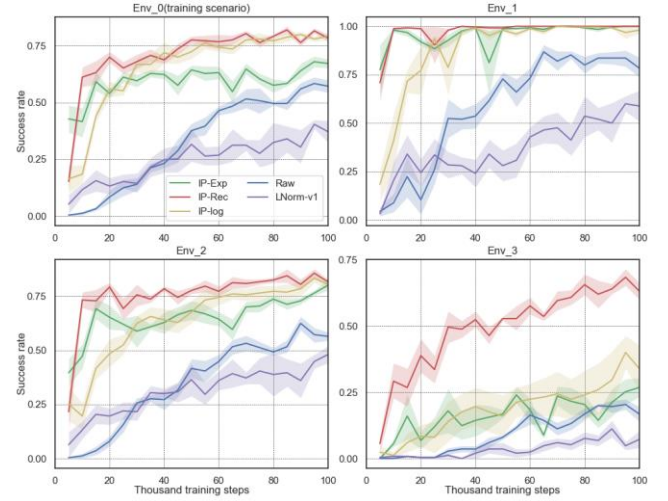


Fig. 8. Average learning curves of DRL agents trained in Env_0 using conventional and IP approaches with fixed hyperparameters. The solid lines represent the success rates, and the translucent areas indicate the variance of scores or success rates in five runs.

As IP-Rec performs the best among all the IP approaches, we use it as the default IP approach in the remaining comparison study. For IP-Rec, the hyperparameter β_i is manually set based on our empirical analysis, which may not be optimal. To find the optimal β_i , we treat it as a trainable variable to automatically learn it from training. We refer to this approach as vi) IP-Rec-Ada: Reciprocal function $\mathcal{P}^R(\cdot)$ with adaptive β_i . Moreover, to evaluate the necessity of the two conditions of IP functions presented in Section IV-A, two NN-based IP functions are compared. Specifically, each IP function has one hidden layer with 128 neurons and their network structures can be found in Fig. 9. As shown, the activation functions used in the two functions are Tanh and ReLU, respectively. As the two functions are NN-based, the learned function may not meet the two conditions of the proposed IP functions. We refer to the two approaches as vii) IP-NN-Tanh: one-hidden-layer NN with Tanh activation functions; viii) IP-NN-ReLU: one-hidden-layer NN with ReLU activation functions.

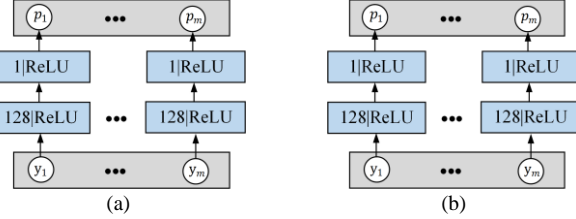


Fig. 9. Illustration of NN-based IP approaches: (a) one-hidden-layer NN with Tanh activation functions; (b) one-hidden-layer NN with ReLU activation functions.

The comparison results of these adaptive IP functions are given in Fig. 10. As shown, IP-Rec-Ada performs better than IP-Rec in the crowded Env_3 and slightly outperforms IP-Rec in the training scenario. IP-NN-Tanh achieves a much higher success rate and learns faster than Raw in Env_0, Env_1, and Env_2, but it performs similarly to Raw in crowded Env_3. To explore the reason behind this result, we plot the function curve learned by IP-NN-Tanh in Fig. 11 and compare it to the IP-Rec function. As shown, IP-NN-Tanh learns to compress the long-distance values, which helps reduce the proportion of long-distance values in the input space and enhances the agent's generalization capability in relatively open scenarios such as Env_1. However, compared to IP-Rec, it fails to expand the range of short-distance values since its function curve is near-linear in the short-distance region. Accordingly, its performance is not improved in Env_3.

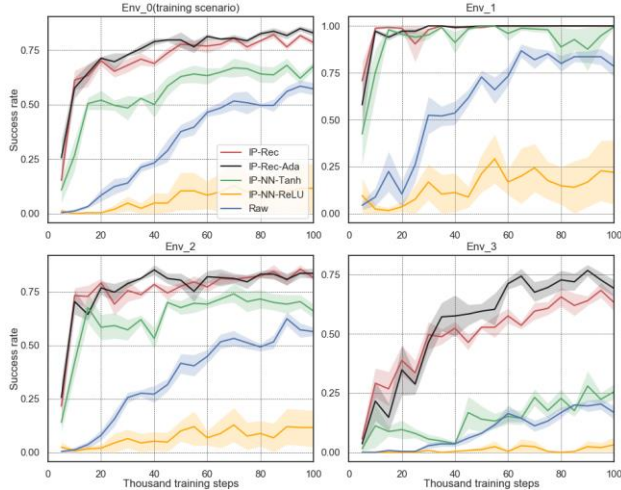


Fig. 10. Average learning curves of DRL agents trained in Env_0 using fixed and adaptive IP approaches.

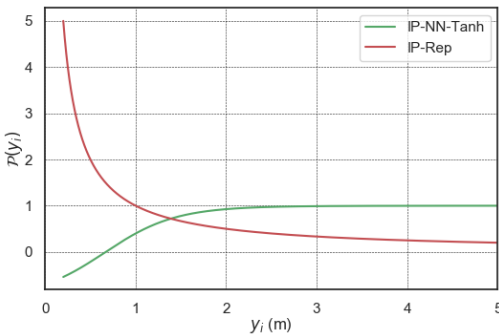


Fig. 11 Function curves of IP-Rec and IP-NN-Tanh.

Last, to further study and compare the navigation performance of the agents, we plot the trajectories of agents trained with Raw, IP-Rec, and IP-Rec-Ada in Fig. 12. The markers used for the different terminal states are red cross (crash), green circle (success), and orange triangle (time out). Initial and goal points are marked with blue and yellow circles, respectively.

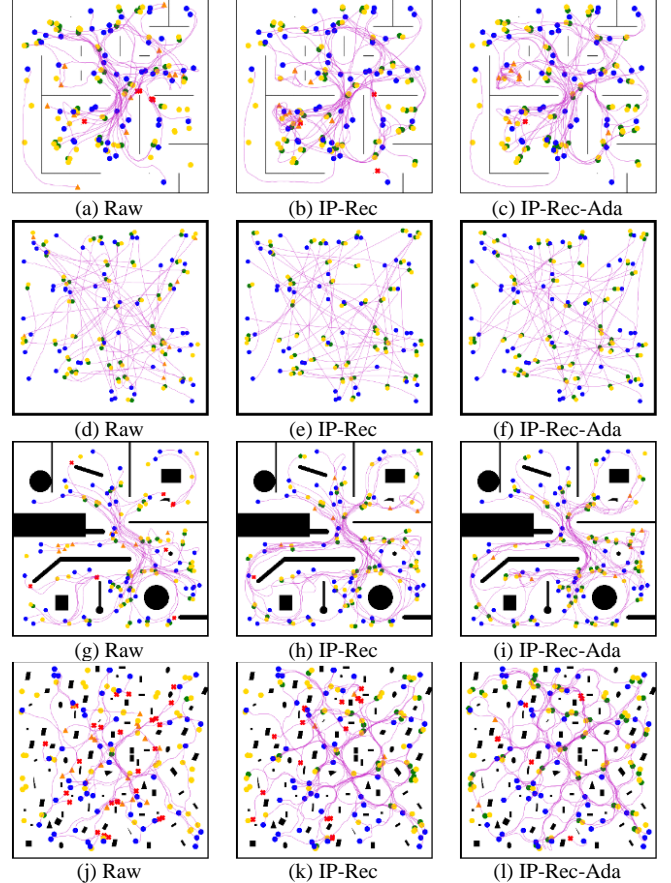


Fig. 12. Trajectories and terminal states visualization of agents trained with Raw, IP-Rec, and IP-Rec-Ada.

As shown, in empty scenario Env_1, the trajectories of agents trained with IP-Rec and IP-Rec-Ada are straighter than the counterparts trained with Raw, while the agent trained with Raw sometimes stop near the goal instead of approaching the goal in Env_1. Moreover, the agent trained with IP-Rec-Ada crashes the least in Env_3, which demonstrates its good obstacle-avoiding capability in crowded scenarios.

B. Case Study Two: Rectangular Robot

In this case study, we evaluate our IP approaches through training a rectangular robot to navigate. As shown in Fig. 13, the training scenario is Env_4 [2], an $8 \times 8\text{m}^2$ crowded room. The rectangular robot used for training has the same size as Pioneer3-DX robot, whose length is 0.455m and width is 0.381m. Different from the previous case, LiDAR is mounted on the front of the robot ($y_l = 0.1\text{m}$, see Fig. 2). Its FOV is 240° , angular resolution is 0.47° (512 laser beams) and scanning range is 5.6m [2]. The speed limits of the robot remain the same as the previous case. The networks used for training the robot are given in Fig. 5(b). The input size of laser scans is reduced to 32 through min-pooling. The initial robot

positions and goal positions are randomly regenerated according to the size of the new robot in Env_3. The rest of the training and testing procedures follow the same procedures described in Section V-A.

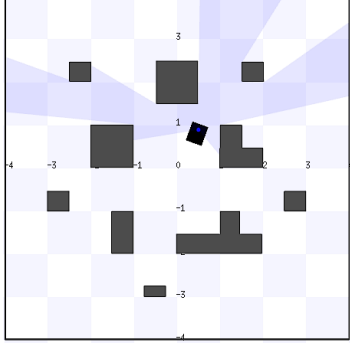


Fig. 13. Env_4: the simulated scenario used for training the rectangular robot.

According to the comparison results in the previous case, in this case study, we only evaluate the best two IP approaches: i) IP-Rec: Reciprocal function $\mathcal{P}_i^{R}(\cdot)$, where $\rho^{Poc}(p_i^R) = 1/3$; ii) IP-Rec-Ada: Reciprocal function $\mathcal{P}_i^{R}(\cdot)$ with adaptive β_i values, where the initial $\rho^{Poc}(p_i^R) = 1/3$. As the robot is rectangular and the LiDAR is not mounted on the robot center, the minimum measuring range D_i^{\min} and its min-pooled value Y_i^{\min} vary with the direction index i (see Fig. 2). Hence, the IP function $\mathcal{P}_i(\cdot)$ is unique on each y_i value. Similar to the first case, we also compare our IP approaches with iii) Raw: raw LiDAR readings as input and iv) LNorm-v2: Linearly normalized LiDAR readings as input adopted in [4], which is as follows,

$$\mathcal{LN}^{v2}(y_i) = \frac{y_i}{Y_i^{\max}} \quad (9)$$

In addition, as adding more hidden layers in DNN can help extract more nonlinear features from the input, to investigate whether such features are as powerful as the pre-processed representations calculated by our IP functions, we train two models with more hidden layers and compare them with our IP approaches. These two models are iv) Raw-4layer: four-layer DNN with raw distance values as input, v) Raw-5layer: five-layer DNN with raw distance values as input. Following the network structures in Fig. 5, both models have 512 neurons in each hidden layer.

The metric used to evaluate the model's performance in testing scenarios is the success rate of 50 runs in each scenario. The learning curves are plotted in Fig. 14. As shown, IP-Rec and IP-Rec-Ada performs similarly and achieves the highest success rates in all scenario. The performance of Raw-4layer and Raw-5layer are similar to Raw, which indicates adding more layers in actor and critic networks does not help extract useful features from the raw LiDAR readings for robot navigation.

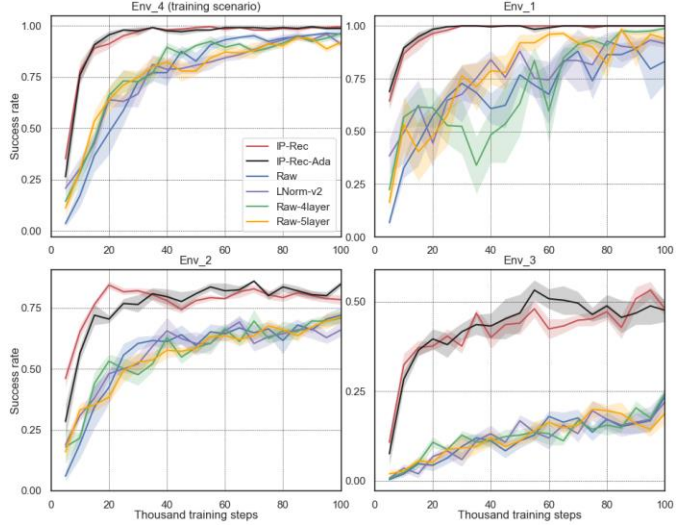


Fig. 14. Average learning curves of DRL agents trained in Env_4 using conventional and IP approaches.

VI. CONCLUSIONS

In this work, we find the conventional input representation of LiDAR readings is the key factor behind this performance degradation of DRL agents in real-world applications. To address this problem, we present IP approaches to highlight the important short-distance values of laser scans and compress the range of less-important long-distance values. Extensive experiments have been carried out, and the comparison results show that the proposed IP approaches can greatly increase the learning speed of the DRL agent and enhance the agent's performance in unseen scenarios.

REFERENCES

- [1] L. Xie *et al.*, “Learning With Stochastic Guidance for Robot Navigation,” *IEEE Transactions on Neural Networks and Learning Systems*, 2020. [Online]. Available: <http://arxiv.org/abs/1811.10756>.
- [2] L. Xie, S. Wang, S. Rosa, A. Markham, and N. Trigoni, “Learning with training wheels: Speeding up training with a simple controller for deep reinforcement learning,” in *Proceedings - IEEE International Conference on Robotics and Automation*, 2018, pp. 6276–6283, doi: 10.1109/ICRA.2018.8461203.
- [3] H. Shi, L. Shi, M. Xu, and K. S. Hwang, “End-to-End Navigation Strategy with Deep Reinforcement Learning for Mobile Robots,” *IEEE Trans. Ind. Informatics*, vol. 16, no. 4, pp. 2393–2402, 2020, doi: 10.1109/TII.2019.2936167.
- [4] L. Tai, G. Paolo, and M. Liu, “Virtual-to-real deep reinforcement learning: Continuous control of mobile robots for mapless navigation,” in *IEEE International Conference on Intelligent Robots and Systems*, 2017, vol. 2017-Sept, pp. 31–36, doi: 10.1109/IROS.2017.8202134.
- [5] F. Leiva and J. Ruiz-Del-Solar, “Robust RL-Based Map-Less Local Planning: Using 2D Point Clouds as Observations,” *IEEE Robot. Autom. Lett.*, vol. 5, no. 4, pp. 5787–5794, 2020, doi: 10.1109/LRA.2020.3010732.
- [6] M. Dobrevski and D. Skočaj, “Adaptive Dynamic

Window Approach for Local Navigation,” *2020 IEEE/RSJ Int. Conf. Intell. Robot. Syst.*, pp. 6930–6936, 2020.

[7] T. Fan, P. Long, W. Liu, and J. Pan, “Distributed multi-robot collision avoidance via deep reinforcement learning for navigation in complex scenarios,” *Int. J. Rob. Res.*, vol. 39, no. 7, pp. 856–892, 2020, doi: 10.1177/0278364920916531.

[8] M. Pfeiffer *et al.*, “Reinforced Imitation: Sample Efficient Deep Reinforcement Learning for Mapless Navigation by Leveraging Prior Demonstrations,” *IEEE Robot. Autom. Lett.*, vol. 3, no. 4, pp. 4423–4430, 2018, doi: 10.1109/LRA.2018.2869644.

[9] D. Yook, T. Lee, and Y. Cho, “Fast Sound Source Localization Using Two-Level Search Space Clustering,” *IEEE Trans. Cybern.*, vol. 46, no. 1, pp. 20–26, 2016, doi: 10.1109/TCYB.2015.2391252.

[10] C. Chen, Y. Chen, Y. Han, H. Q. Lai, F. Zhang, and K. J. R. Liu, “Achieving Centimeter-Accuracy Indoor Localization on WiFi Platforms: A Multi-Antenna Approach,” *IEEE Internet Things J.*, vol. 4, no. 1, pp. 122–134, 2017, doi: 10.1109/JIOT.2016.2628713.

[11] H. Mo, Q. Tang, and L. Meng, “Behavior-based fuzzy control for mobile robot navigation,” *Math. Probl. Eng.*, vol. 2013, 2013, doi: 10.1155/2013/561451.

[12] Z. Liu, X. Li, B. Kang, and T. Darrell, “Regularization Matters in Policy Optimization,” 2019.